

Quantitative Biofractal Feedback Part I – Overview – Biofractals

D. W. Repperger, Ph. D. and Robert L. Ewing, Ph. D.
AFRL, WPAFB, Ohio 45433, USA

daniel.repperger@wpafb.af.mil, robert.ewing@wpafb.af.mil

ABSTRACT

This paper discusses a powerful new application of the Quantitative Feedback Theory (QFT) to a class of problems which are becoming more and more prevalent and may involve fractals or a class of distributed parameter systems. In Part I the predicament of interest is posed within the context of identification/classification of network congestion and its relationship to fractal objects. A review of five constituent disciplines is then conducted to provide the requisite background information. In Part II, the general QFT problem is briefly reviewed. Finally, in Part III, the well-known diffusion problem is analyzed several different ways to provide a common thread between the Parts I and II presented. The diffusion problem involves many similar issues that occur inside the network congestion problem, the fractals concept, and can also be formulated within a QFT framework.

1.0 INTRODUCTION

Quantitative Feedback Theory is an area of controller design that has wide applicability because of its simplicity and intuitive nature yet can deal with issues such as robust stability, target tracking, and disturbance rejection. In this paper, uses of QFT to better understand how to analyze and assess the performance of complex networks and systems from nature and in other applications will be conducted. In many cases this may be characterized as distributed parameter systems. The goal is to better comprehend how such schemes work. For example, it is desired to better quantify how to objectively measure performance, vulnerability, and other attributes that occur in such intricate network systems. For many of these entities, including those in the military, a useful measure of performance is the flow of information through such networks. Vulnerability can then be defined as the sensitivity to flow. The presumption is that a poorly performing network is congested and the flow is slow. A better performing system would have a higher rate of flow. Since flow performance is measured in units of bits/second for information systems, the flow rate times time provides the total number of bits going through the network. This also has analogies to discrete event systems. One can then view the overall task in terms of the bits or discrete events required to actually complete the mission in minimum time. Another way to examine this concept is via the expected time to complete the overall mission being calculated as the ratio of the fixed number of bits divided by the flow rate in bits/second.

Networks are ubiquitous as noted in numerous applications such as electric power grids, financial systems, railroad tracks, water distribution systems, food and medicine allocation procedures, etc. which are co-located and complex in nature. Also, information systems, email systems and nature's way of managing physiology can be characterized by multifaceted networks. On the other hand, some networks can be very destructive. For example, a model of a counter improvised explosive device (IED) network exists for a

successful attack on American forces. The goal for the friendly forces would be, in this case, to take such a network down or cause it to have a high congestion. Another example of an undesirable distributed system would be the well-known sexual network involving the spread of disease such as in HIV. In this case the goal would be to make the flow minimal through the entity resulting in a maximally congested structure. This paradigm represents the reduction of the spread of disease because the flow is minimal. Figure (1) shows a possible visual rendering of a network system of interest that may be presented to a decision maker. In areas where the flow is fast (high bits/sec) it is rendered green. In other areas the flow is slower (yellow) or even more slower (orange) and perhaps completely congested (red color). It is noted in Figure (1) that the areas of higher spectral wavelength have more feedback loops and appear more intricate. When looking at a complex display, this visual rendering adds value to decision makers who immediately need to know, spatially, where the congestion area may be located.

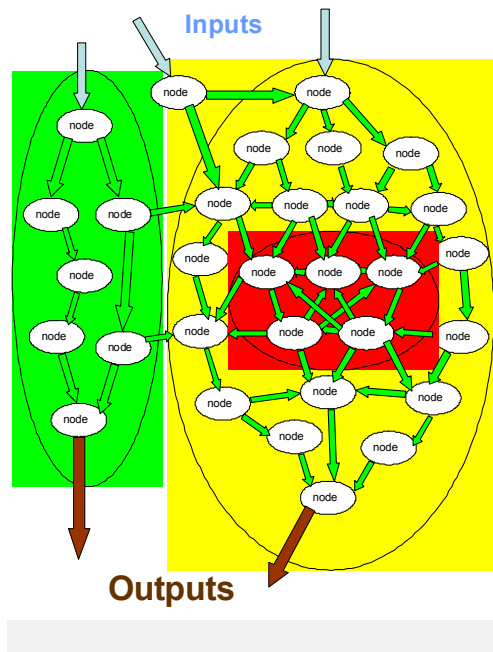


Figure (1) – The Original Network-Centric Distributed System

When controlling complex systems such as in distributed networks, traditional control theory methods may require some modification. For example, linear feedback theory is mainly concerned with transfer functions, which are devised as ratios of outputs to inputs of systems, using as a basis a sine wave time function. The sine wave function has the property that all its derivatives exist and are bounded. Thus the sine wave is a C^∞ function. On the opposite spectrum of continuity, a C^0 function termed the Weierstrass function is introduced herein which has the unique property that it is forever continuous and nowhere differentiable. Figure (2) shows a comparison between these two extreme basis functions (a C^∞ function versus a C^0 function). It is demonstrated later that the C^0 time function (Weierstrass) is also a fractal object enjoying certain optimality properties that may be leveraged in good control system design if flow performance is important. It seems plausible that QFT theory can then be used to analyze objects that may have as a basis function the Weierstrass-like functions as well as those characterized by sine waves. The next section will elaborate on the requisite background of these fractal objects and to develop a framework to analyze them within the context of Quantitative Feedback Theory.

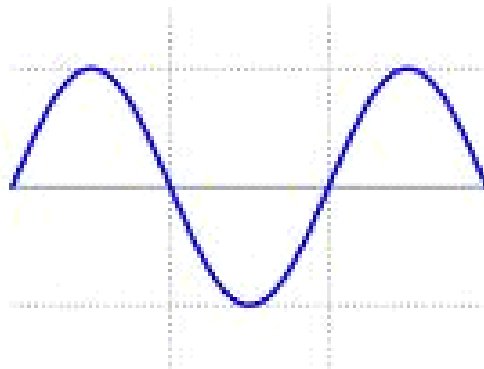


Figure (2a) – A sine wave – A function of the type C^∞

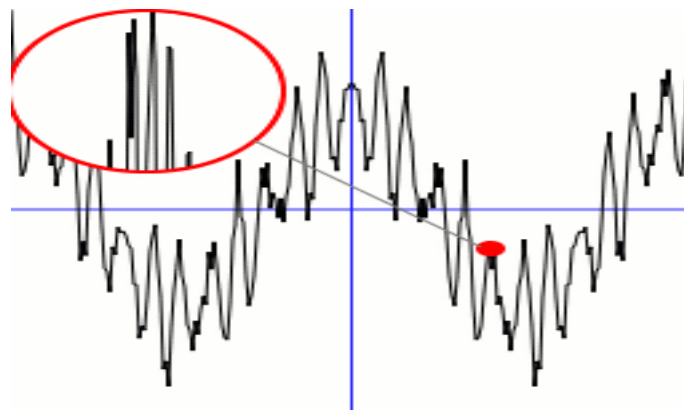


Figure (2b) – The Weierstrass function of the type C^0

To determine visual renderings such as in Figure (1), it is shown in the sequel that the analysis of network performance can be related to the intersection of five areas: optimization theory, graph theory, information theory, fractional calculus, and bioinspired design (fractals). The next section will discuss these five areas, individually, in more detail in the Part I presentation on fractals and bioinspired design.

2.0 PART I – FRACTALS AND BIOINSPIRED DESIGN

Part I of this paper will examine certain related areas involving fractal objects of nature. To better understand how different disciplines interact to shed light on the congested network flow problem, Figure (3) shows the intersection of the five areas of interest that will be discussed, all of which have some relationship to the problem of understanding performance and vulnerability of complex networks.

To summarize, the five areas to be discussed include (1) Bioinspired or fractals, (2) The Fractional Calculus, (3) Information Theory, (4) Graph Theory, and (5) Optimization of a network system. An application from the US military is then worked to show how flow calculations and sensitivity could be determined in a brute force sense. From such an analysis, a robustness paradigm can be determined. With this problem numerically solved, a QFT formulation that can deal with the control of these complex networks is synthesized. The first area to be discussed is termed bioinspired or fractals and raises issues to be addressed in the remainder of this paper.

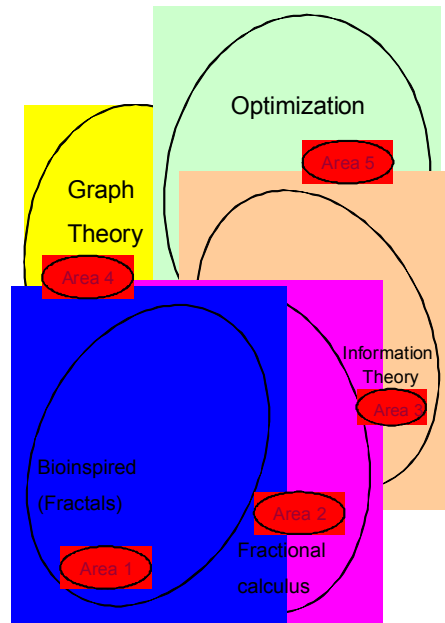


Figure (3) – Five Pertinent Areas to Understand Network Analysis

2.1 Bioinspired or Fractals

From Figure (3), the first of the five areas to be discussed involves bioinspired design or fractals. Fractals are nature’s way of structuring a number of biological entities. Figure (4) portrays some of the better known fractal visual images. Certain fractals can be shown to have dynamics that satisfy the diffusion equation. It follows that there exists a fractional differentiable equation to characterize the flow of these types of systems in nature. To further motivate the approach taken here, Figure (5) shows the optimal diffusion of oxygen in the human lung or the upward diffusion of water in trees. This begs the question on how trees transport water from the roots to the branches and, in a similar manner, why the lung diffuses oxygen in a manner where a fractional dimension comes into play? It can be shown in Figure (5) that the architecture governing optimal diffusion among the constituent branches satisfies the following relationship:

$$(d_1)^\gamma = (d_2)^\gamma + (d_3)^\gamma \quad (1)$$

where $\gamma = 2.5$ for oxygen absorption and is not an integer. This was noted over 500 years ago by Leonardo da Vinci [22]. If γ were an integer representation, such as in equation (1), it would be considered a Euclidean space ($\gamma = 1, 2, \text{ or } 3$). However, if γ is not an integer, this is termed a non-Euclidean space, which is characteristic of fractal objects. The term “fractal” is derived from the Latin word “fractus” which means “broken” or “fractured.” It will be demonstrated that a fractal is scale free (having a self-similar property). Such entities are also forever continuous and nowhere differentiable. For some other example fractals, they may have infinite area and finite volume. In other situations, fractals could have an infinite circumference but finite area. In both cases the higher dimension is finite, but the next lower dimension is not. This has advantages in nature where the goal, for the example of the lung, is that a finite volume exists for the lung, but the distribution (or flow) of oxygen is proportional to the area of the lung surface, which is to be maximized.

Hence, nature selects the fractal architecture for improving flow performance. This provides an optimal distribution system for the flow variable (oxygen, water, blood, etc.), which is desired. Finally, this viewpoint provides a non Euclidean geometric method to view the world, which is vastly understudied. It should be emphasized that fractals are *not minimum energy designs*. Rather, they maximize flow properties which motivates their study in complex networks where performance is very much related to flow characteristics.

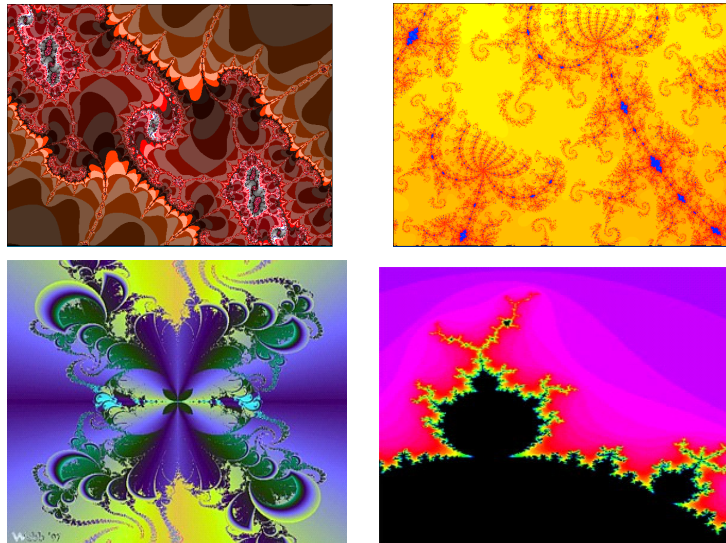


Figure (4) – Four Classical Fractal Objects as Visual Renderings

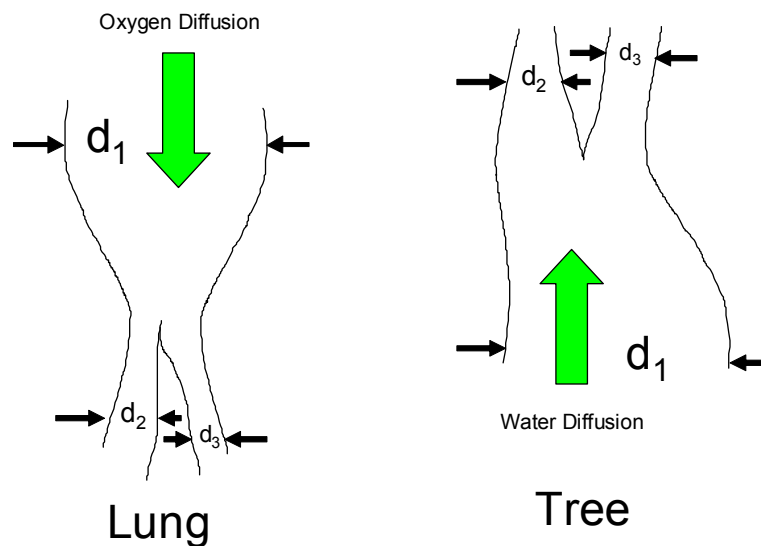
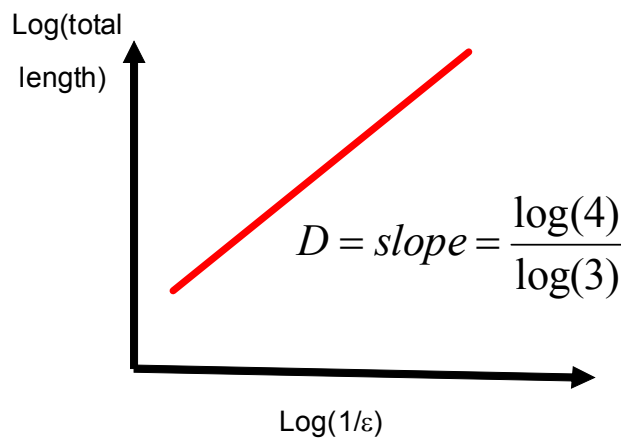


Figure (5) – The Optimal Distribution Problem from Nature (Bioinspired Design)

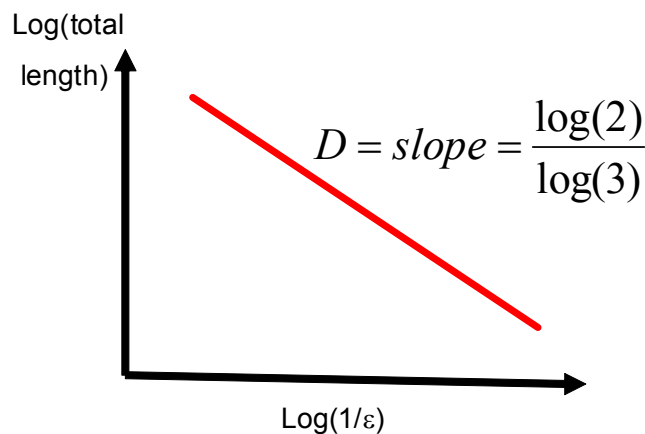
In the study of fractals, originally from B. Mandelbrot [22] the question was raised, “How long is the coastline of Britain?” When measuring the coastline of Britain by a ruler that constantly decreases in size, the logarithm of the total coastal length plotted versus the reciprocal of the ruler length shows a straight line on a log-log plot (similar to the top plot in Figure (6)). This demonstrates the power law or “scale free effect.” The slope of the line in this log-log plot gives rise to the Hausdorff dimension, which may be a non integer. Two examples are now worked to show how this fractional dimension occurs which makes the study of such systems non Euclidian. The first fractal object discussed is the Koch Snowflake which has a fractional dimension of 1.26185... Such a figure is very interesting because it has an infinite circumference and a finite area. In figure (6), the Hausdorff dimension (Hausdorff-Besicovich) D can be defined via:

$$(\text{Total Length}) = L^D \tag{2}$$

where L is the unit basis length and the (Total Length) is the measurement variable (perimeter for objects in a two dimensional framework).



Fractal Example 1– The Koch Snowflake $D = 1.26185\dots$



Fractal Example 2– The Cantor Set, $D = 0.63092\dots$

Figure (6) – The Scale Free Effect Demonstrating Self Similarity

2.1a The Koch Snowflake Fractal

In Figure (7) a description on how to synthesize the Koch snowflake is presented. A line of unity length is divided into 3 parts. For the middle part, an equilateral triangle is then constructed. The total length of the object then increases to 4 units or $(4/3)^n$ where n is the number of times the operation is repeated. Figure (8) starts with an equilateral triangle, as a basis, and repeats the operation on each side indefinitely.

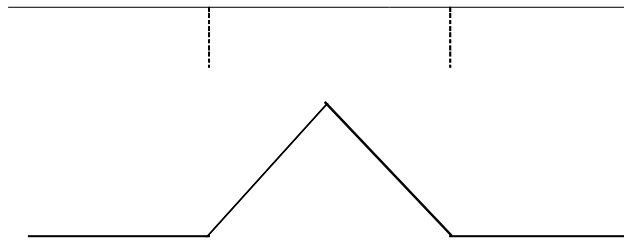


Figure (7) – The Preliminary Construction of the Koch Snowflake

Figure (8) portrays various versions of the Koch Snowflake as $n \rightarrow \infty$ starting with an equilateral triangle. By comparing the total perimeter $= (4/3)^n$ as $n \rightarrow \infty$ demonstrates that the perimeter is unbounded. What is

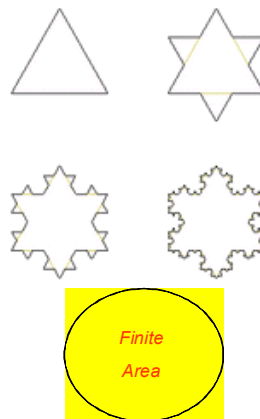


Figure (8) – The Koch Snowflake as $n \rightarrow \infty$

interesting is that the total perimeter is unbounded but the enclosed area of the fractal figure is finite, since the entire object in Figure (8) is bounded within a circle as indicated, the area still remains finite. Returning to

Figure (6), the top diagram is the log of the total length (perimeter) versus $\log(1/\epsilon)$, where ϵ is the ruler length. On a log-log plot, a line of positive slope (Hausdorff dimension of $D = 1.26185.. = [\log(4)]/[\log(3)]$) is greater than one which implies the total perimeter diverges to infinity as $n \rightarrow \infty$. The second fractal object of interest will have a vanishingly small perimeter. From the perspective of having a derivative, a tangent to the limiting diagram in Figure (8) would be forever discontinuous indicating a lack of a derivative.

2.1b The Cantor Set Fractal

The second classical fractal considered is the Cantor set or “Cantor Dust” as noted by Mandelbrot. This object has a fractional dimension of 0.63092... and has the interesting property that the set of deleted points have a Lebesgue measure of 1.0 for an initial interval of length unity. The second fractal set introduced here has a total final length with a Lebesgue measure of 0. Figure (9) shows the Cantor set developed with

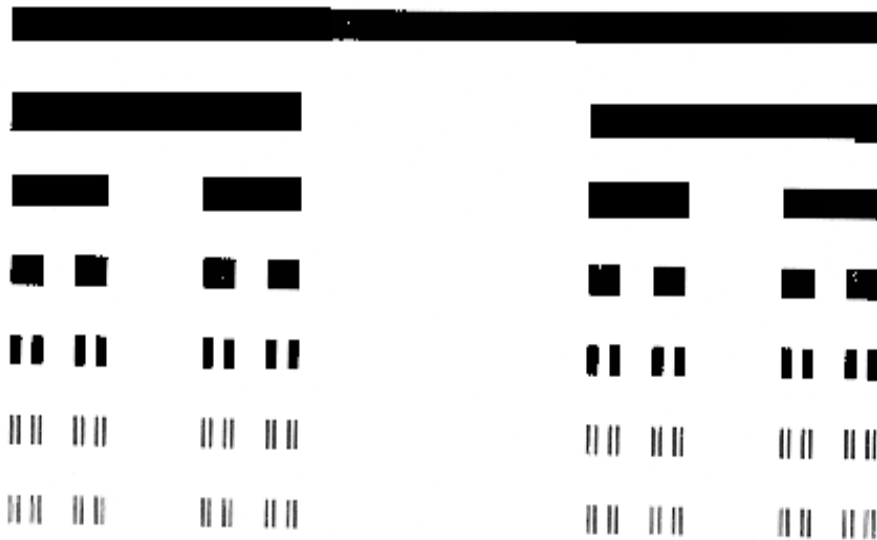


Figure (9) – The Cantor Set as a Fractal Object

the following simple set of rules: The top line in Figure (9) is presumed to have an original length of unity. The middle third of this line is then removed. The total length is then $(2/3)$ times the original line. The process is then repeated with the middle third removed from the lines in the second row in Figure (9). The process is then repeated on the third row, on the fourth row, etc. The overall length becomes $(2/3)^n$ and as $n \rightarrow \infty$ the overall length $\rightarrow 0$. This resulting set is the “Cantor Dust” as described by Mandelbrot. Referring back to Figure (6), the lower diagram plots the total length versus the reciprocal ruler length $(1/\epsilon)$ on a log-log scale. On this log-log plot, a line of negative slope (Hausdorff dimension of $D = 0.63092.. = [\log(2)]/[\log(3)]$) is less than one which implies the total perimeter converges to zero as n increases. It is said the deleted points have a Lebesgue measure of 1.0 and the remaining points (Cantor dust) have a Lebesgue measure of 0. For completeness, a description of how to measure the fractal length, Hausdorff dimension, and other attributes is briefly outlined.

2.1c The Box or Disk Covering Method to Evaluate the Measurement Variable

Fractals also occur in numerous applications in real time data series such as in physiological data, and it is desired to characterize the Hausdorff dimension by empirical means. Hence, the discussion of fractals should also include measurement of the elusive perimeter or length through a box or disk covering methodology. Figure (10) shows how this is accomplished for the Koch snowflake. By inserting disks or boxes around the fractal object, the total length can be determined by summing the disk lengths.

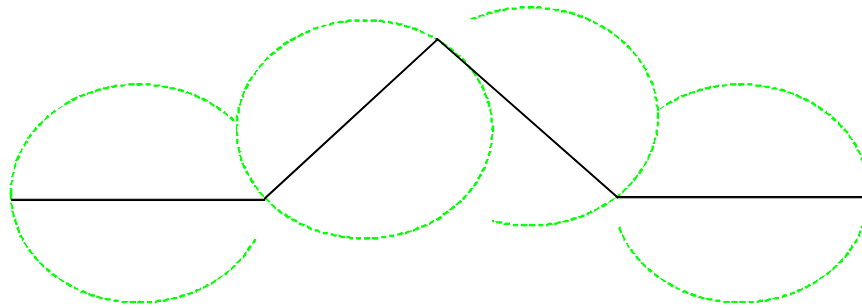


Figure (10) – The Box/Disk Length Counting Method as Applied to the Koch Snowflake Fractal

To show the further applicability of the material presented up to this point, it should be noted that the scale free property of visual fractals can be viewed as a visual image is drilled down (magnify a portion of the image). The magnified image is similar to the original image no matter what degree that portion of the fractal is increased in size. Thus for the Koch snowflake fractal of Figure (8) as the final fractal is magnified at higher and higher powers of amplification, the original fractal shape remains the same.

The fractal objects presented so far have been spatial in a sense but they also may represent temporal data. For time series data, this property is sometimes termed “statistical self similarity”, referring to the real time domain attributes of the information. For example, for real time data, Leland, et al. [20], in Figure (11) is a plot of frequency of messages versus time on the Internet in a dynamic sense, as the time scale decreases logarithmically (for sampling times of $\Delta T = 100, 10, 1, 0.1,$ and 0.01 seconds). Drilling down on any plot (magnifying by changing the ΔT by a factor of $1/10$) yields a time series with a similar shape, which is very analogous to the spatial fractals presented previously. In Figure (12) are data from another study on the Internet, Crovella and Bestavros [6] in which scale free plots were obtained from World Wide Web traffic. These results also extend to a number of physiological systems. In particular, West et al. [7, 35], when plotting the individual heartbeat variability versus time, the graph shows this same statistical self similar property. In Figure (13) from [35], as the magnification of the time series is increased, the same pattern emerges. The box/disk counting method in Figure (10) is ideal for determining the Hausdorff dimension of these types of time series data and classifying the type of fractal that is in the data. To determine the Hausdorff

dimension, for physiological data, the total length of a time series is first determined as in Figure (10). A plot is then constructed with the log of the regressed total length versus the log of the reciprocal ruler length. The slope of this line is the empirical derived Hausdorff dimension.

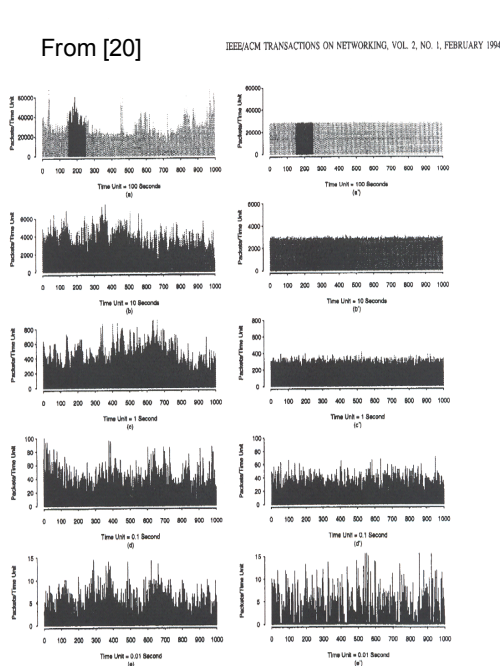


Figure (11) – A Time Series Fractal – Internet Traffic

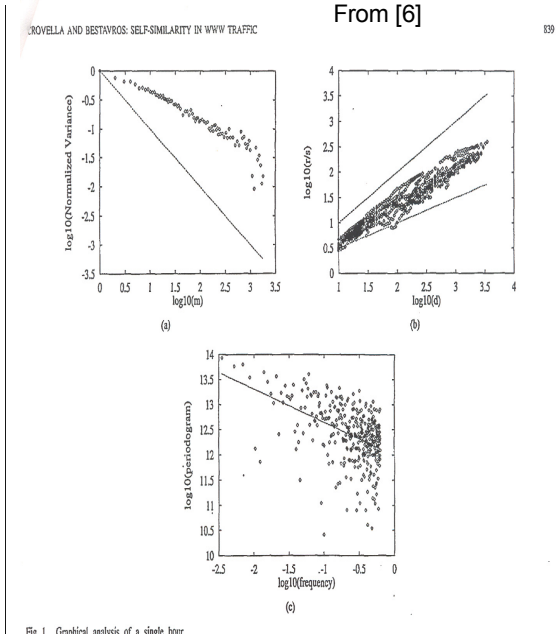


Fig. 1. Graphical analysis of a single hour.

Figure (12) from [6] Showing Scale Free Time Fractals

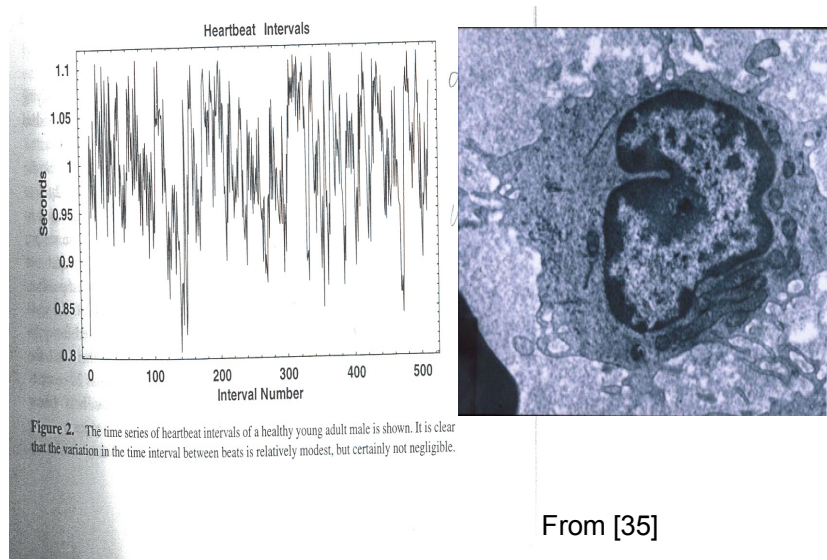


Figure 2. The time series of heartbeat intervals of a healthy young adult male is shown. It is clear that the variation in the time interval between beats is relatively modest, but certainly not negligible.

From [35]

Figure (13) – Physiological Data – Variation of the Time Interval Between Heartbeats

2.2 The Fractional Calculus

The second important topic to relate the five areas of interest in Part I of this paper is the Fractional Calculus, Oldman and Spanier [25]. Over 310 years ago, the mathematician L'Hopital asked Leibniz, the inventor of the notation in equation (3) ($y(t)$ is the output variable and $u(t)$ is the input variable of a physical system) the following question: "Suppose n were not an integer?"

$$\frac{d^n y(t)}{dt^n} = u(t) \quad (3)$$

The response by Leibniz indicated that such a notion was possible, may lead to controversy, but also may add value in new discoveries. Prior and modern work in this area has shown that n may be irrational $n = \sqrt{2}$ or even complex $n = \sqrt{-1}$ and have some utility. A brief motivation on why this field has attracted new attention in modern times is presented next.

2.2a Two Motivations for Modern Studies in the Fractional Calculus

The first motivation for using fractional calculus is related to new research in Materials. In the last 5-10 years, a typical literature search in the areas of fractional calculus shows hundreds of recent hits in the Physics and Materials areas. The motivation for this renewed interest in this field, which also has achieved a high level of rigor, is due to applications in composite materials. In Figure (14) is a picture of a composite material composed of multi layers of different constituent materials. The Bode plot for a transfer function of some output to input variable has a slope which of the form s^{-n} where n is clearly not an integer.

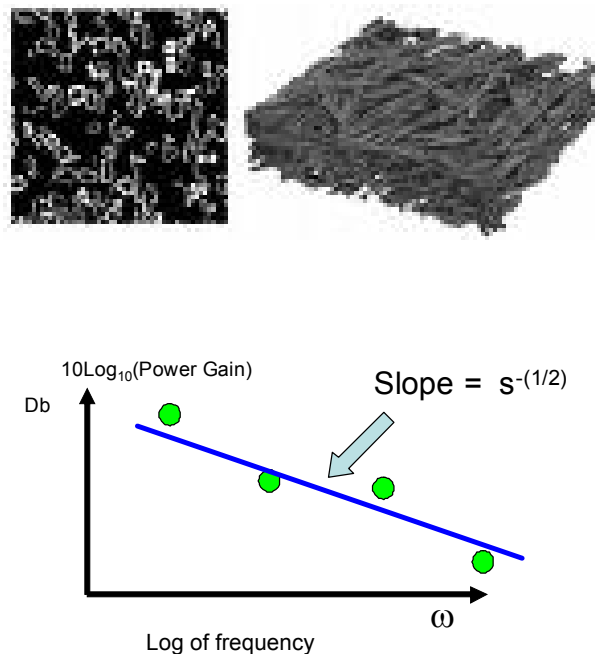


Figure (14) – Composite Materials and a Bode Plot

When composite materials are constructed, there is no reason why the Bode plot slope should be an integer

power (positive or negative) of the Laplace transform variable s . To capture the real time dynamics of the response of such materials in the time domain, it will now be required to have fractional differentiation properties (treating the Laplace transform operator in the sense of a derivative operator).

The second reason why the fractional calculus has achieved a new interest is due to the ability of fractional derivatives to discern the scale free property already discussed for fractal objects. This property is presented in equation (4) without proof but will be discussed shortly:

Scale Free Property of a Fractional Derivative:

$$\frac{d^q f(bx)}{[dx]^q} = b^q \frac{d^q f(bx)}{[d(bx)]^q} \tag{4}$$

In equation (4), the fractal parameter is the term “ b ” and the term “ q ” need not be an integer. This means the fractional derivative is valid over all relative scales and the dynamics remain intact, but only change by a constant factor. This has analogies to the fractal objects in which by drilling down on visual objects, the same figure consistently appears. To show this is equivalent to a power law effect, Moffat, [23] the following definition is noted: “A power law $f(x) = x^a$ has the property that the relative change in:

$$\frac{f(kx)}{f(x)} = k^a \tag{5}$$

is independent of x .” This has the same meaning as equation (4) because the function $f(x)$ lacks a characteristic scale (this is termed “scale free” or “scale invariant”) since it does not depend on x . This is illustrated with an example. Substituting (ky) into $f(y) = y^a$ yields the following steps:

$$\frac{f(ky)}{f(y)} = \frac{(ky)^a}{y^a} = k^a \frac{y^a}{y^a} = k^a \tag{6}$$

Again, from equation (6), since the right hand side does not depend on x or y , this shows the lack of characteristic scale and demonstrates that power law functions **have independence from the x or y scale** which has been illustrated for the fractal objects previously considered. It is now appropriate at this point in time to introduce the Weierstrass function.

2.2b –The Weierstrass Function – A Fractal Time Series – Forever Continuous -Nowhere Differentiable

So far fractal objects have been identified in a spatial and temporal sense in terms of visualizations. Fractal objects also satisfy fractional differential equations. As noted previously, the fractal objects have the attribute that they may be forever continuous and nowhere differentiable. It is appropriate to now introduce the fundamental basis functions for fractals, which has analogies to the sine wave for Euclidean dimensional systems, but has applicability to non Euclidean systems. As originally synthesized by K. Weierstrass in 1872 and presented to the German Academy of Science, equation (7) describes the first version of the Weierstrass function which was proclaimed to be forever continuous but never differentiable at any point.

$$f(x) = \sum_{n=0}^{\infty} a^n \cos(b^n \pi x) \tag{7}$$

where $0 < a < 1$, b is a positive integer and $ab > 1 + (3/2)\pi$ (the original and conservative conditions specified by Weierstrass). The existence of a function that was forever continuous but nowhere differentiable provided a culture shock to the mathematicians at that time, where it was presumed that such a function could never be constructed. Figure (15) shows a plot of a typical Weierstrass function and the same scale free properties appear, as with fractals. This is seen as magnification, of any portion of the curve, reveals the original curve all over again at any level of amplification.

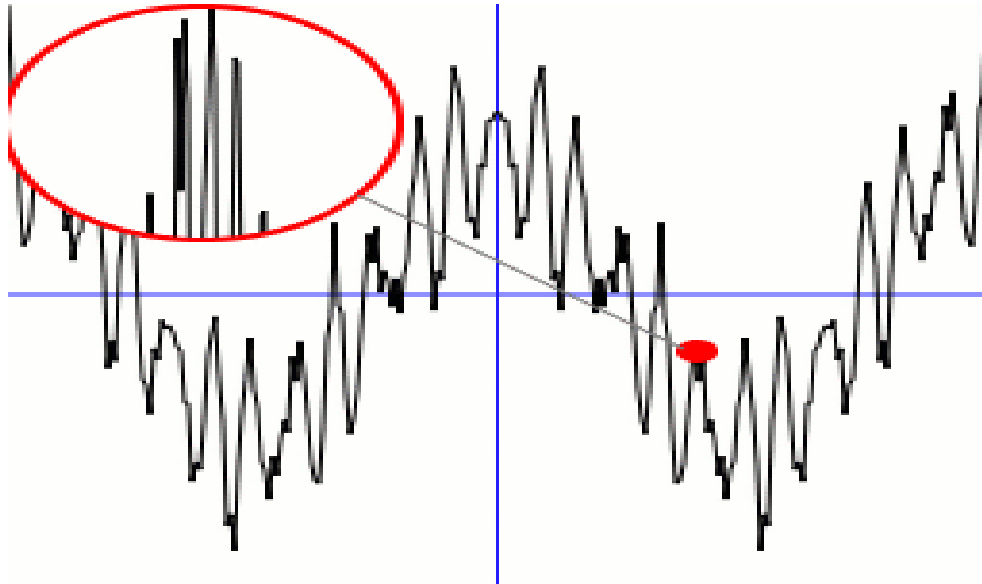


Figure (15) – The Weierstrass Function – A Scale-free Time Series

It is important to explain the *modus operandi* of how K. Weierstrass originally synthesized this function and how it can be used in future applications involving the analysis of systems that have a scale-free property. To understand how a function can be synthesized which is forever continuous but never differentiable, consider the power series representations in equation (8):

$$\sum_{n=0}^{\infty} x^n = \frac{1}{1-x} = 1 + x + x^2 + x^3 + \dots \quad (8)$$

It is obvious that the series converges if and only if $|x| < 1$. This can be viewed within the framework of a radius of convergence in Figure (16). Thus x could be positive, negative or even a complex number and the series in equation (8) will converge if the magnitude of x lies within the unit circle in Figure (16). What Weierstrass did to the function $f(x)$ in equation (7) was to take its derivative as follows:

$$f'(x) = \sum_{n=0}^{\infty} -a^n b^n (\pi) \sin(b^n \pi x) \quad (9)$$

Since the constant factor π can be taken outside the summation in equation (9), requiring $|a| < 1$ can be shown to guarantee convergence of $f(x)$ in equation (7), but specifying the product terms $|a b| > 1$ in equation (9) puts each term outside the radius of convergence of the power series for $f'(x)$. Thus $f(x)$ is well defined but $f'(x)$ will always diverge. Hence a function has been created which is forever continuous (since $f(x)$ is only composed of C^∞ functions of the sine and cosine nature) but $f'(x)$ can never be finite because the series in equation (9) will always diverge. What is most interesting is that the fundamental Weierstrass function in equation (7) starts with C^∞ functions (cosine wave) but ends up with a C^0 time series. A brief description of the fractional calculus methods is presented next with its relationship to the prior work.

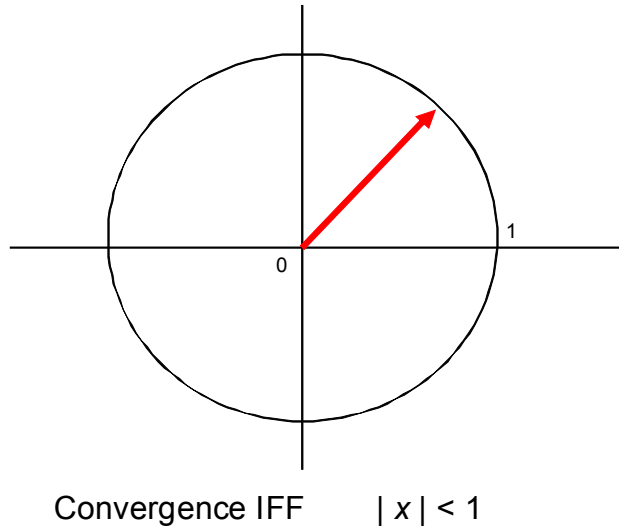


Figure (16) – Radius of Convergence for a Power Series

2.2c – A Brief Introduction to the Fractional Calculus

Since brevity must be the style here, only the salient points with regard to Fractional Calculus are presented with limited rigor. The first step is to define the Gamma function which permits the definition of the factorial function to be generalized to non integers:

Step 1: Define the Gamma Function:

$$\Gamma(z) = \int_0^{\infty} e^{-u} u^{z-1} du, \tag{10}$$

Thus it can be shown that:

$$\Gamma(1) = 1 \tag{11}$$

By integration of parts, it then follows:

$$\Gamma(z + 1) = z\Gamma(z), \tag{12}$$

The key relationship between a factorial function and the Gamma function now results:

$$\Gamma(z + 1) = z!, \tag{13}$$

But z does not have to be an integer in equation (10), for example let $z = \frac{1}{2}$ resulting in the following:

$$\Gamma\left(\frac{1}{2}\right) = \sqrt{\pi} \tag{14}$$

Thus a methodology now exists (via equation (13)) to express factorials of fractional quantities. The second step is to consider fractional derivatives of powers of x^m , for example, where m is an integer:

Step 2: Develop Fractional Derivatives for x^m :

Starting with:
$$\frac{d}{dx} x^m = mx^{m-1} \quad (15)$$

If β were an integer, it would follow that:
$$\frac{d^\beta}{dx^\beta} x^m = \frac{m!}{(m-\beta)!} x^{m-\beta} \quad (16)$$

To generalize this to the case that β may not be an integer would imply from equation (13):

$$\frac{d^\beta}{dx^\beta} x^m = \frac{\Gamma(m+1)}{\Gamma(m-\beta+1)} x^{m-\beta} \quad (17)$$

This is a valid definition for β not an integer, e.g. the following fractional derivative can be easily obtained:

$$\frac{d^{\frac{1}{2}}}{dx^{\frac{1}{2}}} x^1 = \frac{\Gamma(1+1)}{\Gamma(1-\frac{1}{2}+1)} x^{1-\frac{1}{2}} = \frac{2}{\sqrt{\pi}} x^{\frac{1}{2}} \quad (18)$$

Now suppose a function $f_1(x)$ is represented in a power series in x^n , i.e.

$$f_1(x) = \sum_{n=0}^q a_n + b_n x^n \quad (19)$$

Then the fractional derivatives of $f_1(x)$ can be calculated (term by term) using equation (17) and the series has well defined terms. If $q \rightarrow \infty$ in equation (19), the series would converge if the terms a_n and b_n fall within the radius of convergence as specified in Figure (16). The next step is to generalize this concept to functions that are related to e^{ax} .

Step 3: Develop Fractional Derivatives for e^{ax} :

Following the discussion in equations (15-17), define the derivative operator D^v as follows:

$$D^v = \frac{d^v}{dx^v} \quad (20)$$

Then for e^{ax} , the following relationship exists if v is an integer or non integer.

$$D^v e^{ax} = \frac{d^v}{dx^v} e^{ax} = a^v e^{ax} \quad (21)$$

Now suppose a function $f_2(x)$ can be represented as a power series in e^{ax} as follows:

$$f_2(x) = \sum_{n=0}^q a_n + b_n e^{c_n x} \quad (22)$$

It then follows that the function $f_2(x)$ can be differentiated term by term using the relationship in equation (21).

As before, if $q \rightarrow \infty$ in equation (22), the series would converge if the terms a_n , b_n and c_n fall within the region of convergence as specified in Figure (16). Finally these methods can be even further generalized to include all possible trigonometric functions.

Step 4: Develop Fractional Derivatives for $e^{i\theta}$:

Using the well-known Euler relationship (i is a complex number):

$$e^{i\theta} = \cos(\theta) + i \sin(\theta) \tag{23}$$

And the inverse relationships between the trigonometric functions, e.g.:

$$\cos(\theta) = \frac{e^{i\theta} + e^{-i\theta}}{2} \tag{24}$$

Then for any series $f_3(x)$ that can be represented by a Fourier series description such as:

$$f_3(x) = \frac{a_0}{2} + \sum_{n=1}^q a_n \cos(nx) + b_n \sin(nx) \tag{25}$$

Using the relationships in equations (21, 24-25) has a well defined fractional derivative. Again if $q \rightarrow \infty$ in equation (25), the series would converge under appropriate conditions.

Finally it is noted that since $f_1(x)$, $f_2(x)$, and $f_3(x)$ represent most common functions, the fractional derivatives have wide applicability. Incidentally, for the Weierstrass function (defined in equation (7)), the fractional derivatives could also be calculated within an infinite series framework using equation (7). This is a strange situation where the Weierstrass function cannot have a derivative but the fractional derivatives may have an analytical representation in terms of an infinite series, but the well defined series would have a divergence problem.

It should also be noted that the fractional calculus now has a rigorous approach to optimization as presented in [1,2]. The next area to be discussed is related to information theory.

2.3 Information Theory

The next topic (area 3 from Figure (3)) considered involves information-theoretic methods. This has value in the study of flows in complex networks because there is a simple framework between network structures and developing the information flow quantities [28, 29, 31, 34]. From its early history, in 1948, C. Shannon [33] developed a theory of how information can be computed between sources and received signals. Figure (17) represents how the information channels are modelled for the network science problem considered in this paper. One particular variable of interest is the mutual information variable ($I(x;y)$ in Figure (17)), which is defined as the reduction in uncertainty in an input object by observing an output object. Mutual information is interesting because it provides a flow rate (bits/second) which is also amenable to the study of performance in graphs and networks. Another important variable that also provides performance evaluation is the relative information distance variable D_R . These variables are defined as follows:

$$H(x) = \text{The input uncertainty to the channel} \tag{26}$$

$$H(y) = \text{The output uncertainty of the channel.} \tag{27}$$

$$H(x/y) = \text{Equivocation lost to the environment.} \tag{28}$$

$$H(y/x) = \text{Spurious uncertainty from the environment} \quad (29)$$

$$I(x;y) = \text{Mutual information transmitted} \quad (30)$$

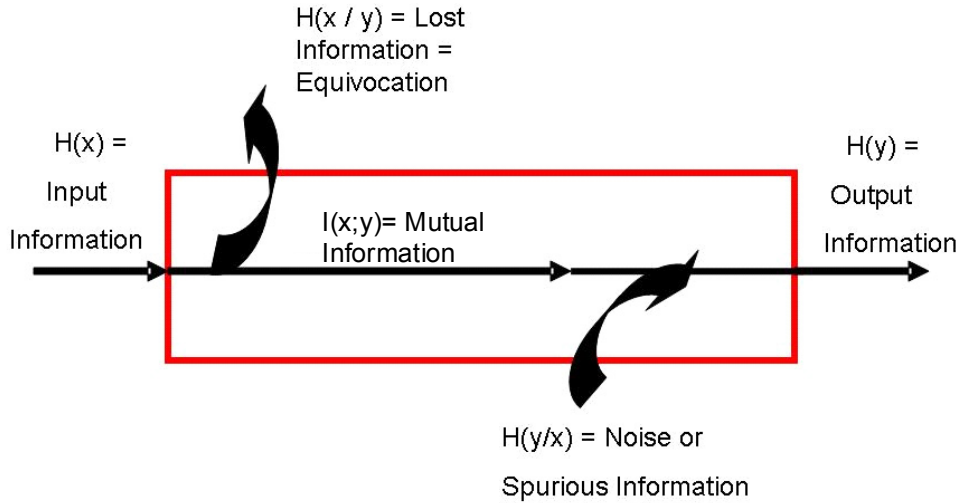


Figure (17) – The Classic Information Channel and Constituent Quantities

More specifically, the details of equations (26-30) can be better described by letting $p(\cdot)$ represent the probability of an event. For an information channel with input symbol set $x \in X$, of size n , and received symbols $y \in Y$ at the output set of size q (q may not equal n), the following entropy ($H(\cdot)$) relationships can be defined:

$$H(x) = \sum_{i=1}^n p(x_i) \log_2(1/p(x_i)) \quad (31)$$

$$H(y) = \sum_{j=1}^q p(y_j) \log_2(1/p(y_j)) \quad (32)$$

$$H(x,y) = \sum_{i,j}^{n,q} p(x_i, y_j) \log_2(1/p(x_i, y_j)) \quad (33)$$

$$H(x/y) = \sum_{i,j}^{n,q} p(x_i, y_j) \log_2(1/p(x_i | y_j)) \quad (34)$$

and

$$H(y/x) = \sum_{i,j}^{n,q} p(x_i, y_j) \log_2(1/p(y_j | x_i)) \quad (35)$$

It can then be shown to be true (Cover & Thomas [5]) that:

$$I(x;y) = H(x) + H(y) - H(x,y) \quad (36)$$

where the mutual information $I(x;y)$ satisfies (which is appropriate as a flow variable in networks):

$$I(x;y) \geq 0 \quad (37)$$

Finally, another key variable that is useful is the relative information distance D_R defined as follows:

$$D_R = H(x/y) + H(y/x) - H(x) - H(y) = 2I(x;y) \quad (38)$$

where D_R also has a similar property, as in equation (37):

$$D_R \geq 0 \quad (39)$$

There are special properties and advantages that variable D_R provides over $I(x;y)$ which are known in the literature [5] and restated here without proof:

Property 1: D_R satisfies the requisite properties of a metric; however $I(x;y)$ is only a positive measure. Please see [30] for a counter example where $I(x;y)$ fails as a metric.

Property 2: The relative information distance metric D_R is the complement of $I(x;y)$, (cf. [31]) i.e.

$$D_R(x;y) = \bar{I}(x;y) \quad \text{or} \quad I(x;y) = \bar{D}_R(x;y) \quad (40)$$

The utility of using information theory constructs to evaluate performance in complex networks can be summarized by the following four salient points:

(P-1) The Units of $I(x;y)$ or $D_R(x;y)$:

The units of $I(x;y)$ and $D_R(x;y)$ are both bits/second. Using $I(x;y)$, the total bits would be the product term ($I(x;y) * \Delta T$) where ΔT is the task completion time. Thus to complete the total bits through a system, it would take, on average, ΔT seconds as a measure of task performance. This definition can also be applied to D_R , but it is not as lucid.

(P-2) Minimum Time Corresponds to Maximum $I(x;y)$ and Vice Versa:

From the previous point, the critical time to complete a task can now be written:

$$\Delta T = \frac{\text{Bits}}{I(x;y)} \quad (41)$$

Thus if $I(x;y)$ is maximized, and the bits are fixed, then the critical time is minimized. Thus a minimum time scenario could be characterized as a maximization of the mutual information $I(x;y)$ flow rate. Also from equation (41), to maximize the time to complete a task, then the goal would be to minimize $I(x;y)$.

(P-3) The Analogy to Discrete Event Systems

If the completion of the mission requires a number of discrete event tasks to be accomplished, then equation (41) may be modelled via:

$$\Delta T = \frac{\text{Total Task Events}}{I(x;y)} \quad (42)$$

If bits and events can be related, $I(x;y)$ may be interpreted as having units of events/second and from equation (42), the maximization of $I(x;y)$ will provide optimal minimum time performance. The minimization of $I(x;y)$ will provide worst case maximum time performance, which may be the desired outcome for a hostile network.

(P-4) Optimal Flow Performance and an Attack Paradigm to Congest a Network

From equation (42) and the prior discussion on adversarial networks, the strategy that produces the minimal $I(x;y)$ provides a paradigm and strategy to attack a network or reduce its efficacy. One can view the nodes, such as in Figure (1) as control variables to be manipulated to adjust the overall flow vector (set of network flows) that will adjust the overall mutual information flowing through the network.

The fourth area of interest from Figure (3) refers to Graph theory, which is pertinent to better understand the architecture of networks which has a considerable influence on performance, vulnerability, and constraints in complex distributed systems.

2.4 Graph Theory

Graph theory is fourth area of discussion from Figure (3) which relates to the characteristics of the architecture of complex systems. The distinction is first made here between a random graph and a scale free graph. Many modern graphs tend to have an architecture similar to scale free graphs (“the rich get richer philosophy”) and they are compared here to the random graph architecture. Of course, other types of graph structures exist but they are not elaborated on in this paper.

2.4a – The Architecture of a Random Graph

A random graph or Erdős-Rényi graph [18] can be constructed by having approximately the same number of links between the nodes. A simple example is the land highway system in the USA where the major cities have about the same number of links (major highways) between each major city (left plot in Figure (18) from [18]). In Figure (18) the term random graph means that the distribution of the number of links (x axis) follows a normal curve with the mean of the density as the most common number of links between nodes. This framework is sometimes called a thin tail distribution.

2.4b – The Architecture of a Scale-free Graph

A scale free graph means that a power law relationship would exist for the same plot as in Figure (18) for the random graph (number of nodes with k links versus number of links). This is typical of the airline routes, as displayed in Figure (18) on the right most plot. In this case there are many nodes with a small amount of connections and a few key nodes with many connections, which is typical of airline routes with central hubs. There are many common networks that are considered to have a scale-free architecture such as the Internet as displayed in Figure (19). In this instance, as new links are added, the most highly connected nodes more likely gain additional links, which is the “rich get richer” concept. This framework is sometimes called a fat tail distribution because on a linear plot such as Figure (18) on the right, the tail is much higher to the right as compared to the random graph case. Figure (20) shows additional evidence of the scale free property of the Internet, Faloutsos, Faloutsos, and Faloutsos [10]. A short discussion on different types of vulnerability of the various graphs is pertinent.

2.4b.1 Vulnerability Aspects of the Different Graph Structures

Vulnerability has different interpretations with respect to the two types of graphs previously discussed, which is also dependent on the type of network attack. For example, for a random graph, it is less vulnerable to a focused attack on any one node in comparison to a scale-free graph. For the scale free graph, however, the focused attack is much more effective if it is directed against a highly connected node. If the

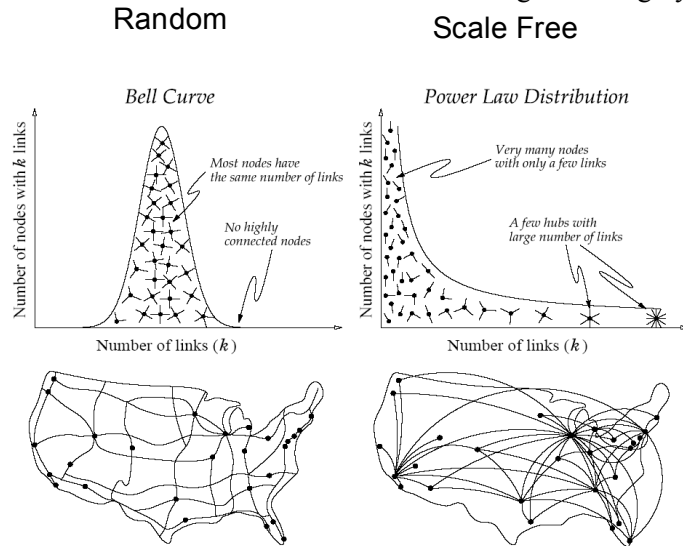


Figure (18) – Random Graphs versus Scale-free Graphs for Transportation Systems

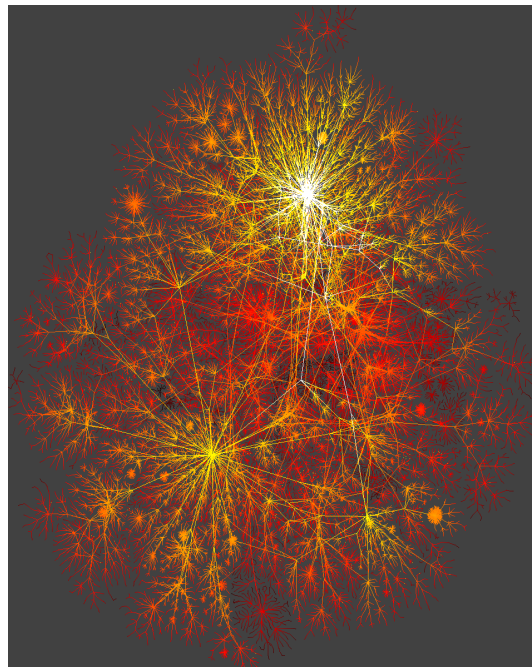


Figure (19) – The Internet – A Scale-free Graph

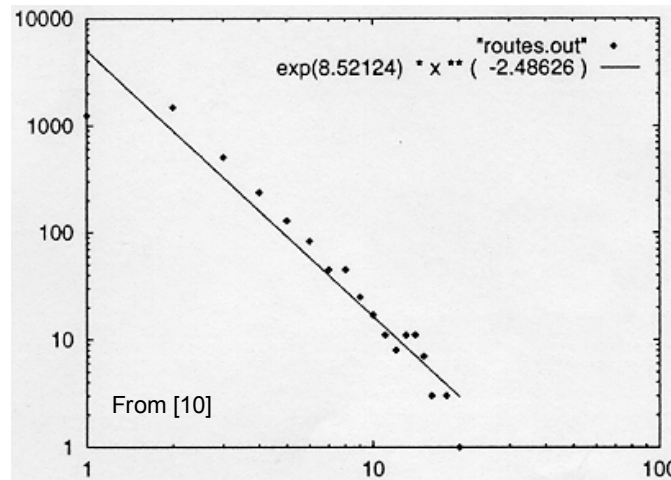


Figure (20) – Evidence of the Internet being Scale-free in Structure

type of attack is random (a node is selected at random), then the scale-free graph is less vulnerable. This is because, on the average, the nodes with the fewest connections, will more frequently be attacked (there are many more of these nodes), which has a reduced effect. For the random graph and the random attack, all nodes are equally probable of being compromised and the overall effect on the network’s performance will be about the same. A short discussion on the constraint relationships that may arise for the flows through a network also arise from graph theory constructs and the architecture employed.

2.4c.1 Constraint Relationships That Exist in Graph Theory

Figure (21) displays the concept of a “cut set” that occurs in Graph Theory. The cut set is used in

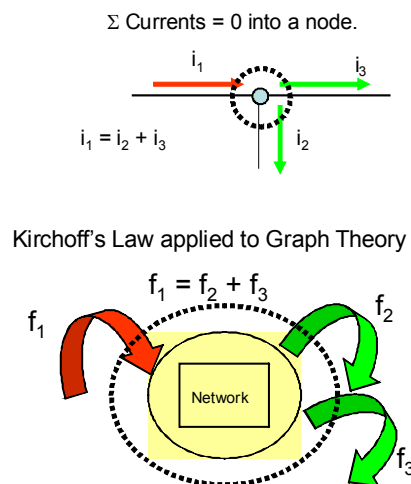


Figure (21) – Kirchoff’s Law in Circuits and Networks

electrical circuit theory and the top diagram shows the analogy to the Kirchoff's current laws in which the sum of currents into a node must sum to zero. It is a statement that flows cannot be created or destroyed and they must be accounted for. A cut set is a closed curve. All flows that enter a cut set must leave the cut set unless a source or sink of flows resides inside the cut set. If a source or sink falls within a cut set, then the sum of the flows is adjusted, accordingly, to include the values of the source or sink.

The fifth and last topic mentioned in Part I discusses an example of a network which could be worked via a brute force computational method. It demonstrates the ability to identify sensitivity and performance using a computationally intelligent method.

2.5 Optimization of a Network System

An example is now worked regarding a well-known air-logistics network in US Air Force applications. The problem is formulated in terms of graph theoretic means with the unknown vector of flows to be determined. This is equivalent to using the nodes to manipulate the flows and this begs the question of what set of flows maximizes the overall network performance and also what other set of flows may minimize the overall network's performance? Using principals from Graph Theory, such as Kirchoff's Law, a set of constraints is determined from the cut set laws (application of Kirchoff's Law). A sensitivity function is defined in the sequel as the rate of change of cut set flow to the total network's mutual information flow. Using genetic algorithms in a computational performance study, the flow vectors are then determined which maximize and minimize the overall total network's mutual information flow. The sensitivity function is then easily calculated for any nodes or sets of nodes through the cut set. The sensitivity of the different nodes is determined and examined.

First, a description of an air logistics system is presented, Lyons, Repperger, and Seyba, et al. [21, 31, 32]. The flow performance optimization is conducted on an air logistics model by utilizing genetic algorithms [26,27].

2.5a – The Air Logistics System

The air logistics system considered in this paper represents all the tasks required to refresh an aircraft after it has landed. This includes removing the passengers and cargo, cleaning the aircraft, uploading new cargo and passengers in the proper sequence. The five key players in Figure (22) are the ATOF (the overall coordinator), the PS (passenger services), the CS (cargo services), FS (fleet services), and RS (ramp services). Each of these players has key roles that have to occur in a proper time sequence. The goal of this optimization study is to determine the optimum communications between the key players. The flow arrows are the communications. In Figure (22) is the architecture of the minimum possible communications scenario where the ATOF only talks back and forth individually with each of the other four players. The goal is to find the optimum amount of communications. Too little or too much communications may not be appropriate. In Figure (23) is the opposite extreme where all players could talk with each other, whether or not it is necessary. The first step is to define the initial architecture between the two extremes of Figure (22) and Figure (23).

2.5b – The Architecture Issue

The first step is to define a reasonable architecture (number of flow arrows to be obtained) with too few links (Figure (22)) and, perhaps, too many links (Figure (23)) which are to be optimized for overall network performance. Links refer to communications between nodes. Studies were run with human subjects (Lyons [21], Repperger, et al. [30, 31], Seyba, et al. [32],) to determine the initial architecture. Figure (24) is the finally selected architecture which seemed to evolve from the study with human subjects indicating that certain types of communications were very pertinent, yet other types of communication were probably not

necessary. There are now 15 unknown flows $[f_1, f_2, \dots, f_{15}]$ in Figure (24) that need to be determined. It is noted that the vector f_x represents an exogenous input/output flow of aircraft through the network and acts like a forcing function. For example five aircraft could arrive every hour, so f_x would be the input and output of the network in terms of $f_x = 5$ aircraft/hour.

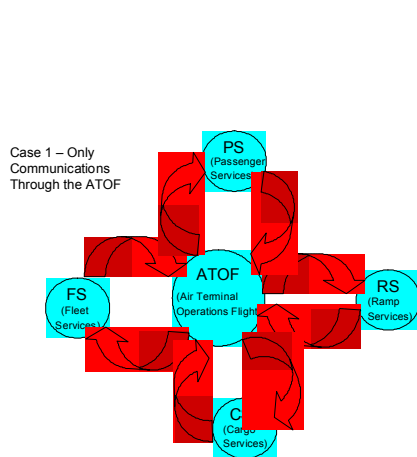


Figure (22) – The Air Logistics System – Minimum Communications

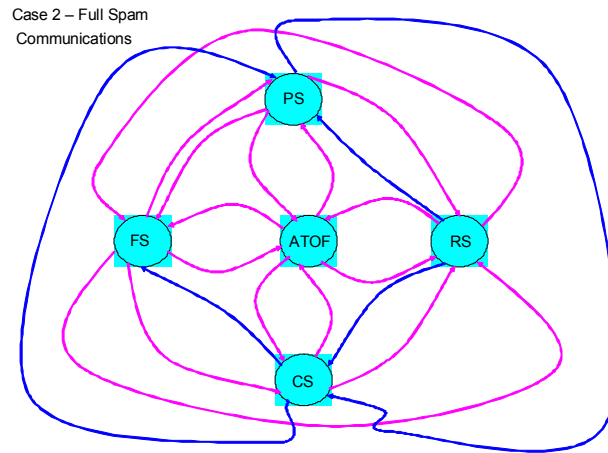


Figure (23) – The Air Logistics System Maximum Communications

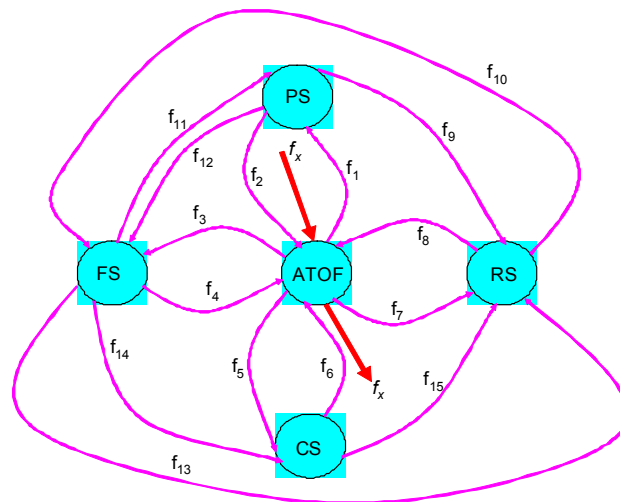


Figure (24) – The Air Logistics System – The Final Architecture Selected

2.5c – Formulating the Optimization Problem – Find the Flow Vector

In Figure (24), the 15 flows $[f_1, \dots, f_{15}]$ need to be determined. From the architecture selected in Figure (24), certain architecture constraints must exist on these 15 flows. Using Kirchoff's Law with a cut set around each of the five nodes, the following constraint equations result:

$$\begin{aligned} \text{ATOF: } f_x + f_2 + f_4 + f_6 + f_8 &= f_1 + f_3 + f_5 + f_7 + f_x & (43) \\ \text{PS: } f_{11} + f_1 &= f_9 + f_2 + f_{12} & (44) \\ \text{RS: } f_{15} + f_7 + f_9 + f_{13} &= f_{10} + f_8 & (45) \\ \text{FS: } f_{10} + f_{12} + f_3 &= f_{14} + f_{13} + f_4 + f_{11} & (46) \\ \text{CS: } f_5 + f_{14} &= f_{15} + f_6 & (47) \end{aligned}$$

The optimization problem can now be formulated as follows:

Given that the flow f_x is fixed and constant, find the optimal flow vector $[f_1, f_2, \dots, f_{15}]$ that satisfies the constraints in equations (43-47) and optimizes a cost function based on the mutual information through the overall network of Figure (24). The two optimization problems are specified for the cost function J_I :

$$J_I = I(x;y) \text{ of the network in Figure (24) for } f_x \text{ fixed} \quad (48)$$

Optimization Problem 1: Find the optimal vector $[f_{1a}, f_{2a}, \dots, f_{15a}]$ to **maximize** J_I subject to the constraint equations (43-47) and a fixed f_x .

Optimization Problem 2: Find the optimal vector $[f_{1b}, f_{2b}, \dots, f_{15b}]$ to **minimize** J_I subject to the constraint equations (43-47) and a fixed f_x .

A computational approach will be employed to obtain the solutions to the two optimization problems posed above.

2.5c – Formulating the Genetic Algorithm (GA) Approach to Find the Optimal Flow Vectors

The formulation of the GA problem consists of 3 steps:

Step 1: Generation of the Chromosome

From Figure (24), there are 15 possible flows to be optimized. However, from equations (43-47), there are 5 constraints (4 of which are independent). The remaining 11 flows represent the set of flows that needs to be determined.

Step 2: The Fitness Function:

From equation (48), the calculated overall network's mutual information ($I(x;y)$) is the fitness function, determined from the network in Figure (24) subjected to the five constraint equations (43-47).

Step 3: Initial Conditions on the Flow Variables

In the initiation of the optimization procedure, an admissible set of flow parameters is required. After some work, the following initial conditions on the flow variables were selected, which satisfy the constraints in equations (43-47): $f_1 = 3, f_2 = 1, f_3 = 2, f_4 = 2, f_5 = 2, f_6 = 4, f_7 = 3, f_8 = 3, f_9 = 1, f_{10} = 3, f_{11} = 1, f_{12} = 2, f_{13} = 1, f_{14} = 3, f_{15} = 1$.

Some other issues in this computational study involve the construction of the chromosomes to identify each flow f_i . Since there are 11 unknown flows, the granularity of the flow variable will be determined by the number of bits in each chromosome. Since the maximum flow could be as much as 7 units, as seen in the initial conditions set, a 3 bit word (presuming integers for flow variables $f_i \leq 7$ was assumed). Figure (25) displays a class of possible chromosomes for the 11 independent flow variables that must be determined.

$j = 1, \dots, 11$ free chromosomes
3 bit word for each chromosome.

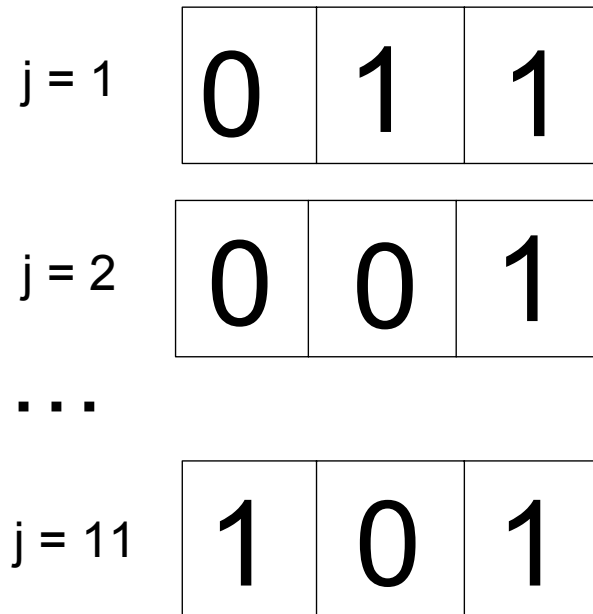


Figure (25) – Construction of the Chromosomes for each flow.

2.5.c.1 Computational Complexity of the Simulation

From Figure (25), each flow can take on up to eight possible values (2^3). Since there are 11 unknown flows, the total number of possible combinations is 8^{11} which is prohibitive to determine in a computational sense. Thus a combinatorial nightmare is quickly discovered (NP-complete problem) beyond the capability of most practical computers. Hence genetic algorithms were selected to address this problem.

2.5.c.2 Criteria for the Fitness Pool

A pool of 20 chromosomes of the optimum J_l values is developed. This is termed the “elite pool.” Two types of optimum J_l values are determined (largest $I(x;y)$ or lowest $I(x;y)$) on two different computer simulations. New individual chromosomes are created from the elite pool by using the standard GA operations of crossover (to preserve good qualities) and mutation (to include diversity). The ratio of mutation to crossover operation was 1/6, which is a little higher than the typical standard in the literature.

2.5.c.3 Convergence Criteria and Computation Time

The “elite pool” is initially filled up with 20 identical flows based on the admissible initial conditions. As new chromosomes are created, the fitness function value is calculated. The 20 individuals in the elite pool are then rank ordered in terms of fitness. If the new chromosome has a level of fitness better than the least

optimal member of the elite pool, the new chromosome replaces the former member of the elite pool. This process is continued until either the elite pool converges to the same flow values or if a fixed number of iterations are reached (e.g. 10,000 iterations). The most fit members (with the optimal J_I values) are considered as the final members of the pool and represent the optimum solution for that amount of computational effort. Two separate computer simulations were conducted to see the difference in the optimum solutions of minimum or maximum flow rate (minimum or maximum $I(x;y)$ values).

2.5.c.4 – Results and Discussion

Figures (26) and (27) portray a statistic related to the mutual information ($I(x;y)$) versus entry number into the elite pool for the case of maximization and minimization of mutual information. From an efficiency point of view, it took 168 hours of computation time on a personal computer for each plot, thus this is a brute force approach. The ratio of best to worst case mutual information flow shows over a 400% difference in overall network performance.

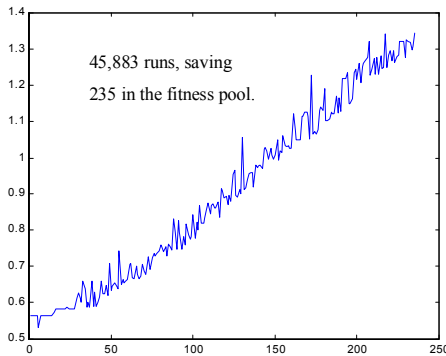


Figure (26) – Maximization of J_I , the Mutual Information of equation (48).

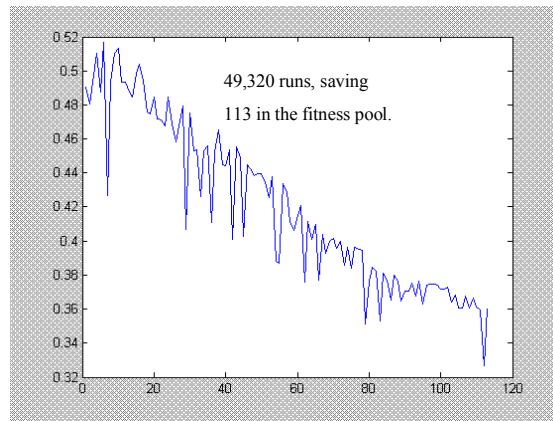


Figure (27) – Minimization of J_I , the Mutual Information of equation (48)

2.5.c.5 – The Vulnerability/Sensitivity Definition

The last remaining portion of this study is to develop a measure of vulnerability/sensitivity of a network. It was seen in the prior section that over a 400% change in network performance can be achieved by modulating the flow vector $[f_1, \dots, f_{15}]$. To derive a measure of sensitivity of performance of a network, consider an arbitrary cut set around some nodes in a network as depicted in Figure (28):

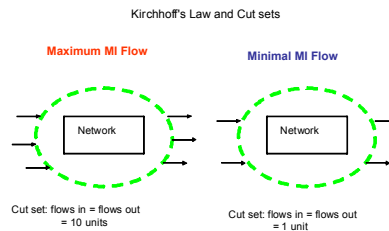


Figure (28) – A Framework for Defining Network Sensitivity/Vulnerability

In Figure (28), the cut set on the left indicates a set of nodes that are evaluated when the overall network has a maximum level of mutual information flow $I(x;y)$. For the network on the left, let T_1 represent the cut set flow (sum of the flows into and out of that particular cut set) and W_1 represent the total mutual information flow in the overall network ($W_1=I_1(x;y)$). For the same physical cut set on the right, when the overall mutual information $I_2(x;y)$ is minimized, let T_2 be the new cut set flow and W_2 the new level of mutual information. If definitions are made of the form:

$$\Delta T = T_1 - T_2 \tag{49}$$

and
$$\Delta W = W_1 - W_2 = I_1(x;y) - I_2(x;y) \tag{50}$$

Then an appropriate definition of sensitivity/vulnerability is provided by S_w^T defined as follows:

$$S_w^T := \lim \frac{\frac{\Delta T}{T}}{\frac{\Delta W}{W}} = \frac{\partial T}{\partial W} \frac{W}{T} \tag{51}$$

For the following reasons:

- (1) ΔW is never zero using the genetic algorithm procedure in which the optimization is not complete until two different levels of mutual information are obtained.
- (2) From Figure (28), if a cut set of nodes has low sensitivity (near zero in magnitude) between the extreme conditions of maximum and minimum overall mutual information flow, these nodes cannot be important in the causality of the network. Conversely, if the cut set of nodes has a large change in cut set flow between the maximum and minimum mutual information flow conditions, then these candidate nodes are more causal and the presumption is that they directly affect the vulnerability.

2.5.c.6 – The Vulnerability/Sensitivity Results

Using the definition of sensitivity/vulnerability in equation (51), the absolute value of S_w^T from equation (51) was calculated for 10 optimizations of the network in Figure (24). A cut set around the most connected node (ATOF) was evaluated versus a lesser connected node (PS). The hypothesis, as usually occurs in graph theory investigations, is that the more highly connected node (ATOF) is probably more vulnerable than a lesser connected node (PS). This is also consistent with the discussion on vulnerability with respect to scale free networks. Figure (29), [31], shows the results of this simulation. It demonstrates that in using this sensitivity measure the consistent result that more intricate nodes are probably more vulnerable or sensitive.

This concludes the Part I work with respect to bioinspired design and fractals. Next, QFT is discussed.

3.0 REVIEW OF THE QUANTITATIVE FEEDBACK THEORY

As an introduction to Part 2 of this paper, the history of the birth of QFT (quantitative feedback theory) is brought to light. Starting with the work in the early 1960's, I. Horowitz developed seminal works originating from the 1970's to introduce the QFT method [13, 14, 15]. It has been now applied in the areas of flight control, power systems, unmanned air vehicles, and in numerous other applications Houppis, et al. [16,17]. A review of work from modern data bases indicated a wide range of important applications [3, 4, 8, 9, 11, 12, 19, 24, 36, 37]. The basics of how QFT is applied are discussed to convert the problem of sensitivity of plant variations and robust control to a method amenable to the classical control area will first be presented.

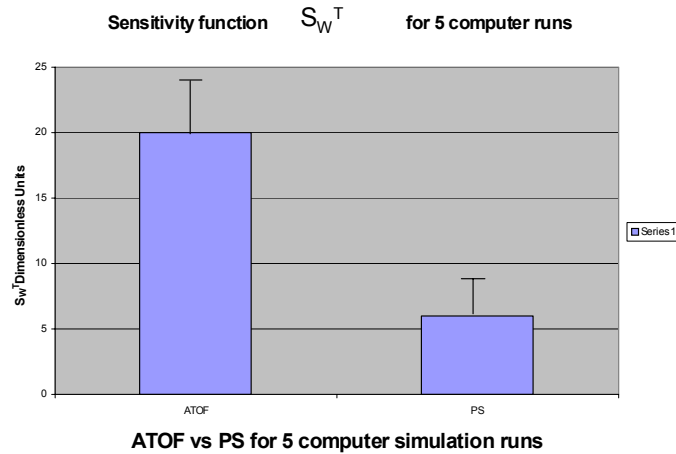


Figure (29) – Results of the 5 Sensitivity Simulations

3.1 Some Basics of QFT

Figure (30) shows the basic three-degree-of-freedom QFT design problem. The controller is $C(s)$

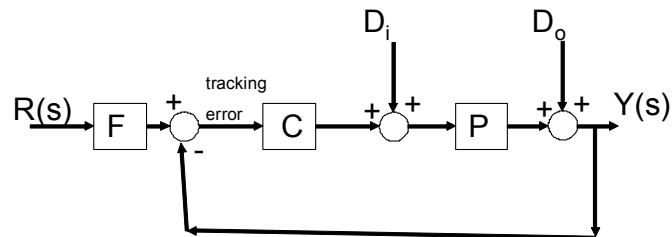


Figure (30) – The QFT Design Problem Formulation

which needs to be determined, the plant $P(s)$ is specified, the input is $R(s)$ with output $Y(s)$, and the input disturbances D_i and D_o affect the tracking error performance. The three requirements for QFT design are robust stability, reference tracking and disturbance rejection, which are quantified in control theory terms. To specify these requirements more concisely, from Figure (30) define the loop gain $L(s)$ as follows:

$$L(s) = C(s) P(s) \quad (52)$$

Then the closed loop transfer function (no disturbances) between the output $Y(s)$ and $R(s)$ is specified via:

$$\frac{Y(s)}{R(s)} = T(s) = \frac{F(s)L(s)}{1+L(s)} = \frac{\text{Output}}{\text{Input}} \quad (53)$$

From classical control theory (Houpis, et al. [17]), the sensitivity of the closed loop transfer function $T(s)$ to the plant variations $P(s)$ can be specified via:

$$S(s) = \frac{\frac{\partial T}{T}}{\frac{\partial P}{P}} = \frac{1}{1+L(s)} \quad (54)$$

Then the three main requirements of QFT can be specified via:

- (1) **Robust Stability:** (closed loop Robust Stability):

$$\left| \frac{L(s)}{1+L(s)} \right| \leq \gamma \quad (55)$$

This provides a constraint on the peak magnitude of the closed loop frequency response.

- (2) **Reference Tracking:** Let T_L and T_U be the lower and upper transfer function, then the requirement is that:

$$|T_L(j\omega)| \leq |T(j\omega)| \leq |T_U(j\omega)| \quad (56)$$

- (3) **Disturbance Rejection:** For closed loop tracking error, a weighting function $W(j\omega)$ is selected such that:

$$\left| \frac{1}{1+L(j\omega)} \right| \leq \frac{1}{W(j\omega)} \quad (57)$$

It is noted that the three conditions above refer to a special class of plants $P \in \{P_i\}$. For the two types of disturbances in Figure (30) (the plant input disturbance D_i and the plant output disturbance D_o), they are specified via the following two transfer functions:

The transfer function between the plant input disturbance D_i and Y which is provided via:

$$T_{di} = \frac{Y(j\omega)}{D_i(j\omega)} = \frac{P(j\omega)}{1+L(j\omega)} \quad (58)$$

and the transfer function between the plant output disturbance D_o and Y is given by:

$$T_{do} = \frac{Y(j\omega)}{D_o(j\omega)} = \frac{1}{1+L(j\omega)} \quad (59)$$

Then the two disturbance rejection conditions can be specified via:

$$|T_{di}| \leq B_{di} \quad (60)$$

$$|T_{do}| \leq B_{do} \quad (61)$$

where B_{di} and B_{do} are frequency dependent functions that can be specified *a priori*.

This brief description of the QFT is sufficient at this point in time. The methodology will be applied to a diffusion problem when placed within the context of a closed loop control system problem. It is helpful to review the history of the heat equation.

4.0 THE COMMON PROBLEM TO BE STUDIED – THE DIFFUSION EQUATION

Figure (31) displays a version of the classical heat equation. Let $u(x,t)$ represent the temperature

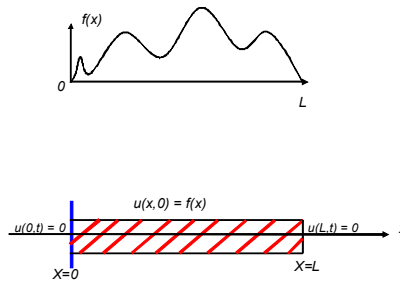


Figure (31) – A Classical Heat or Diffusion Problem

distribution in a cylindrical bar of finite length L oriented along the x -axis and perfectly insulated laterally. The assumption is that the heat flow is only in the x direction. The temperature $u(x,t)$ satisfies:

$$\frac{\partial^2 u(x,t)}{\partial x^2} = a^2 \frac{\partial u(x,t)}{\partial t} \quad (62)$$

with initial condition:

$$u(x,0) = f(x) \quad (63)$$

and boundary conditions:

$$u(0,t) = 0 = u(L,t) \quad \forall t > 0 \quad (64)$$

where a of equation (62) satisfies:

$$a^2 = \frac{c\delta}{k} \quad (65)$$

and the thermal conductivity is k , c is the specific heat with δ as the linear density (mass/ unit length).

Before formulating the QFT problem, it is instructive to review the solution of equation (62) by three

different approaches.

4.1a Solution of the Diffusion Equation via the Fourier Method

The first solution follows the separation of variable approach, as introduced by J. Fourier.

Assume:
$$u(x, t) = X(x)T(t) \quad (66)$$

where $X(x)$ and $T(t)$ are assumed to be separate functions, which have to be determined. Substituting equation (66) into equation (62) yields:

$$a^2 X(x)\dot{T}(t) = T(t)X''(x) \quad (67)$$

Which implies:
$$\frac{a^2 \dot{T}(t)}{T(t)} = \frac{X''(x)}{X(x)} = \text{constant} = -\lambda \quad (68)$$

This must be a constant since it cannot depend on either t or x .

Hence:
$$\dot{T}(t) = -(\lambda / a^2)T(t) \quad (69)$$

Which implies:
$$T(t) = Ae^{-(\lambda/a^2)t} \quad (70)$$

and:
$$X''(x) = -\lambda X(x) \quad (71)$$

Thus:
$$X(x) = B \sin(\sqrt{\lambda}x) + C \cos(\sqrt{\lambda}x) \quad (72)$$

But from the boundary condition:
$$u(0, t) = 0 \Rightarrow C = 0 \quad (73)$$

From the second boundary condition:
$$u(L, t) = 0 \forall t \Rightarrow \sqrt{\lambda} = \frac{n\pi}{L} \quad (74)$$

Hence each $u_i(x, t)$ satisfies:
$$u_i(x, t) = T_i(t)X_i(x) \quad (75)$$

and $u(x, t)$ is the result of the summation of the $u_i(x, t)$ terms.
$$u(x, t) = \sum u_i(x, t) \quad (76)$$

Which implies:
$$u(x, t) = \sum_{n=1}^{\infty} D_n \left(\sin\left(\frac{n\pi x}{L}\right) e^{-\frac{(n^2 \pi^2 t)}{(a^2 L^2)}} \right) \quad (77)$$

The Fourier coefficient D_n satisfies:
$$Dn = \frac{2}{L} \int_0^L f(x) \sin\left(\frac{n\pi x}{L}\right) dx \quad (78)$$

And the infinite series in equation (77) can be shown to converge under appropriate conditions. The second approach to solve the heat equation will be through Laplace transforms.

4.1b Solution of the Diffusion Equation via the Laplace Transform Method

A slightly modified example will be considered. Let the temperature variable $u(x, y)$ satisfy:

$$\frac{\partial^2 u(x,t)}{\partial x^2} = \frac{\partial u(x,t)}{\partial t} \quad (79)$$

with initial conditions: $u(x,0) = f(x)$ (80)

The boundary conditions are replaced by: $u(x,t)$ bounded for $t > 0$, and $-\infty < x < \infty$. (81)

Recall, the Laplace Transform of a function $g(t)$ is specified via: $G(s) = L[g(t)] = \int_0^{\infty} g(t)e^{-st} dt$ (82)

which is permitted under the following conditions: $e^{-at} |g(t)| \leq M < \infty$ (83)

For this distributed system, the following definition is then appropriate for the Laplace transform of $u(x,t)$:

$$U(x,s) = \int_0^{\infty} e^{-ts} u(x,t) dt \quad (84)$$

Laplace transforming the time derivative term in equation (79) yields:

$$\int_0^{\infty} e^{-ts} \frac{\partial u}{\partial t} dt = sU(x,s) - u(x,0) = sU(x,s) - f(x) \quad (85)$$

using the initial condition $f(x)$ from equation (80). If the spatial terms $\frac{\partial u}{\partial x}$ and $\frac{\partial^2 u}{\partial x^2}$ are bounded and continuous, it then follows that:

$$\int_0^{\infty} e^{-st} \frac{\partial^2 u}{\partial x^2} dt = \frac{\partial^2 U}{\partial x^2} \quad (86)$$

The Laplace transform operator is then applied to the entire equation (79) resulting in:

$$L\left[\frac{\partial u}{\partial t} - \frac{\partial^2 u}{\partial x^2}\right] = sU(x,s) - f(x) - \frac{\partial^2 U}{\partial x^2} = 0 \quad (87)$$

Now treating $f(x)$ as a forcing function, equation (87) can be solved as an equation in x as follows:

$$U(x,s) = \frac{1}{2\sqrt{s}} \int_{-\infty}^{+\infty} e^{-\sqrt{s}|x-y|} f(y) dy \quad (88)$$

To find $u(x,t)$, it is now required to obtain the inverse Laplace transform of equation (88):

$$u(x,t) = L^{-1}[U(x,s)] \quad (89)$$

or:
$$u(x,y) = L^{-1}\left[\frac{1}{2\sqrt{s}} \int_{-\infty}^{+\infty} e^{-\sqrt{s}|x-y|} f(y) dy\right] \quad (90)$$

This can be accomplished by integration in the complex plane [25] which can be obtained as follows:

$$u(x,t) = \frac{1}{\sqrt{2\pi t}} \int_{-\infty}^{\infty} e^{-(x-y)^2/4t} f(y) dy \quad (91)$$

A third way to look at the solution of the heat equation is through a fractional calculus framework.

4.1c Solution of the Diffusion Equation via the Fractional Calculus Method

The methods of the Heaviside Operational Calculus can be outlined in the following. Starting with the appropriate version of the heat equation:

$$\frac{\partial^2 u(x,t)}{\partial x^2} = a^2 \frac{\partial u(x,t)}{\partial t} \quad (92)$$

With initial condition:
$$u(x,0) = f(x) \quad (93)$$

and boundary conditions:
$$u(0,t) = 0 = u(L,t) \quad (94)$$

If the time derivative in (92) is replaced by the derivative operator:
$$p = \frac{\partial}{\partial t} \quad (95)$$

And treating p as a constant yields one of two possible ways to solve the resulting equation in the space variable x :

$$\frac{\partial^2 u}{\partial x^2} = a^2 pu \quad (96)$$

Solving (96) in terms of x yields:
$$u(x,t) = Ae^{-ap^{1/2}x} + Be^{ap^{1/2}x} \quad (97)$$

But B must equal zero from the boundary conditions in equation (94) resulting in:

$$u_i(x,t) = e^{-axp^{1/2}} u_0 \quad (98)$$

Again using an infinite series, $u(x,t)$ can be expressed:

$$u(x,t) = u_0 + \sum_{n=1}^{\infty} \frac{(-ax)^n}{n!} p^{n/2} u_0 \quad (99)$$

And the positive, integer, powers in (99) can be replaced by the exponent term $e^{(\cdot)}$. The fractional powers describe an infinite series fractional differential equation. The solution of (99) can be shown to converge to:

$$u(x,t) = u_0 - \frac{2u_0}{\sqrt{\pi}} \int_0^{\frac{ax}{2\sqrt{t}}} e^{-\xi^2} d\xi \quad (100)$$

Alternatively, equation (96) could be solved for $u(x,t)$ directly in terms of p having square root terms which provides a different means of characterizing the diffusion equation within the context of a fractional differential equation.

To conclude this paper, the diffusion equation is now formulated within the context of a QFT control problem to bring these constituent areas together in a single application.

5.0 THE DIFFUSION EQUATION VIEWED WITHIN THE CONTEXT OF QFT

As a common thread to the prior areas presented, a classical thermal regulation problem is examined to show similarities of the heat control problem to the QFT method. Figure (32) provides a formulation to the heat control problem which is amenable to a QFT analysis.

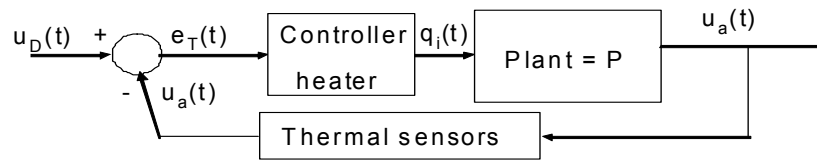


Figure (32) – A Heat Control Problem

In Figure (32) the variables of interest are defined via: $u_D(t)$ is the desired temperature (the presumption is that a spatial slice has been taken in the distributed system ($x = \text{constant}$), and $u_a(t)$ is the actual temperature). The temperature error $e_T(t)$ is the difference between the desired temperature $u_D(t)$ and the actual temperature $u_a(t)$, which is obtained from the temperature sensors in Figure (32). The thermodynamic heat equation governing the relationship between the actual temperature $u_a(t)$ and the heat input q_i is described by:

$$C \frac{du_a}{dt} = q_i - q_0 \tag{101}$$

Where the thermal resistance R_T is related to q_0 as follows:

$$q_0 = \frac{u_a}{R_T} \tag{102}$$

and from a units perspective, the above variables have the following physical dimensions:

All $u_i(t)$ variables have units of degrees centigrade.

The thermal capacitance C in equation (101) has units of kilo-calories/ degree centigrade.

The q_i terms in equations (101-102) have units of kilo-calories / second

The thermal resistance R_T has units of degrees centigrade seconds / kilo calories.

To derive the equations of motion of the plant, equation (101) can be written:

$$C \frac{du_a}{dt} + q_0 = q_i \quad (103)$$

Substituting for q_0 of equation (102) yields:

$$C \frac{du_a}{dt} + \frac{u_a}{R_T} = q_i \quad (104)$$

Multiply through by R_T yields:

$$R_T C \frac{du_a}{dt} + u_a = R_T q_i \quad (105)$$

Laplace transforming with zero initial conditions yields the transfer function to describe the plant dynamics:

$$\frac{U_a(s)}{Q_i(s)} = \frac{R_T}{1 + (R_T C)s} \quad (106)$$

Thus the controller is to be designed is for a first order plant dynamics: To recapitulate a list of the design goals, a QFT controller is specified as follows:

QFT Design Goals:

Goal 1: For stability it is required that the closed loop system $T(s) = \frac{L}{1+L}$ to be stable.

Goal 2: For Tracking Specifications, the prefilter $F(s)$ in Figure (30) is designed to satisfy:

$$|T_L(j\omega)| \leq |F(j\omega) T(j\omega)| \leq |T_U(j\omega)| \quad (107)$$

For specified upper ($T_U(j\omega)$) and lower ($T_L(j\omega)$) bounds on the tracking performance specifications.

Goal 3: For disturbance rejection, it is desired to reject disturbances via $\max |T_{D_i}(j\omega)| \leq |M_{D_i}(j\omega)|$

Where for the input disturbance D_i in Figure (30):
$$T_{D_i} = \frac{P}{1+L} \quad (108)$$

And for the output disturbance D_o in Figure (30):
$$T_{D_o} = \frac{1}{1+L} \quad (109)$$

QFT Design Procedure:

In the QFT Design procedure, the following five step process is then employed:

Step 1: Using the Nichols chart find the admissible set of plant templates $P \in \{P_i\}$.

Step 2: From the Nichols chart, generate the performance bounds: $L_0(s) = P_0(s) G(s)$.

Step 3: For loop shaping, now add poles and zero to $L_0(s)$. This is now called $\bar{L}_0(s)$.

Step 4: Design the Prefilter F to keep $|T_L| \leq |F T| \leq |T_U|$ from equation (107).

Step 5: Finally, to design the final controller, select $G(s)$ to satisfy:

$$G(s) = \frac{\bar{L}_0(s)}{P(s)} \tag{110}$$

5.1 Designing the Final QFT Control System:

When comparing Figure (32) to the proposed QFT controller, Figure (33a) results. It indicates that the controller needs an output that feeds into a plant network consisting of flow variables. The plant becomes the network system of interest. The appropriate controller output should have units related to flow/unit time such mutual information $I(x;y)$ which is bits/sec. For the input to the controller, a difference signal between an actual output and a desired output should be compared. Since the plant dynamics are first order (some integration occurs), one would suspect a viable output of the plant should be related to the integral of the $I(x;y)$ value. From the prior discussion in section (2.3) of this paper, a proper output variable could be either bits or events. From this discussion, the bottom plot in Figure (33b) shows such a possible scenario. The input error to the controller may be an error with units of bits or events, which is consistent with the output of the plant dynamics. The input to the plant dynamics (output of the controller) should have units similar to mutual information.

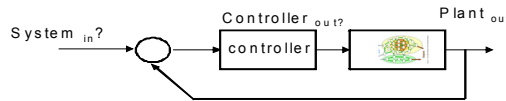


Figure (33a) – The Structure of the Proposed QFT Controller

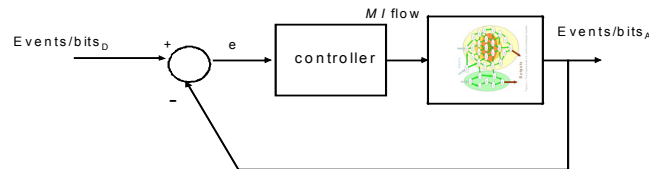


Figure (33b) – The Final Proposed QFT Controller

6.0 CONCLUSIONS

A problem involving network performance, vulnerability, and other issues is studied under various contexts. In Figure (33b) the final controller architecture is proposed that would also be amenable to QFT analysis. It is noted that the role of the controller is to have an error signal input in terms of bits or events and manipulate the mutual information flow output. Recall from section (2.5.c.4) this was precisely the procedure followed when designing the controller via the maximum and minimum mutual information flow. By adjusting the flow vectors, is equivalent to manipulating the knobs in the network, such as in Figure (1).

ACKNOWLEDGEMENT

This work has been supported by US Air Force Grant 231354HC entitled, “Complexity of Glyphs and Systems” funded by the AFOSR.

REFERENCES

- [1] O. P. Agarwal, “Formulation of Euler-Lagrange Equations for Fractional Variational Problems,” *J. Math. Analysis and Applications*, **272**, (2002), pp. 368-379.
- [2] R. Ahmad El-Nabulsi, “Necessary Optimality Conditions for Fractional Action-Like Integrals of Variational Calculus with Riemann-Liouville Derivatives of Order (α, β) ,” *Mathematical Methods in Applied Science*, **vol 30**, issue 15, 2007, pp. 1931-1939.
- [3] D. E. Bossert, G. B. Lamont, M. B. Leahy, and I. M. Horowitz, “Model-Based Control with Quantitative Feedback Theory,” *Proceedings of the 29th IEEE Conference on Decision and Control*, 1990, pp. 2058-2063.
- [4] S. G. Breslin and M. J. Grimble, “Longitudinal Control of an Advanced Combat Aircraft using Quantitative Feedback Theory,” *Proceedings of the 1997 ACC*, pp. 113-117.
- [5] T. M. Cover and J. A. Thomas, *Elements of Information Theory*, John Wiley & Sons, Inc. 1991.
- [6] M. E. Crovella and A. Bestavros, “Self-Similarity in World Wide Web Traffic: Evidence and Possible Causes,” *IEEE/ACM Transactions on Networking*, **5**(6), December, 1997, pp. 835-846.
- [7] W. Deering and B. J. West, “Fractal Physiology,” *IEEE Engineering in Medicine and Biology Magazine*, June, 1992, pp. 40-46.
- [8] D. S. Desanj and M. J. Grimble, “Design of a Marine Autopilot using Quantitative Feedback Theory,” *Proceedings of the ACC*, 1998, pp. 384-388.
- [9] R. L. Ewing, J. W. Hines, G. D. Peterson, and M. Rubeiz, “VHDL-AMS Design for Flight Control Systems,” *Proceedings of the IEEE 1998 Aerospace Conference*, March, pp. 223-229.
- [10] M. Faloutsos, P. Faloutsos and C. Faloutsos, “On power-law relationships of the Internet topology,” *Proceedings of the conference on Applications, technologies, architectures, and protocols for computer communication*, 1999, pp. 251-262.

- [11] M. Garcia-Sanz, I. Egana and M. Barreras, "Design of quantitative feedback theory non-diagonal controllers for use in uncertain multiple-input multiple-output systems," *IEE Proceeding. Control Theory Applications*, **Vol. 152**, No. 2, March, 2005, pp.177-187.
- [12] G. Hearns and M. J. Grimble, "Quantitative Feedback Theory for Rolling Mills," *Proceedings of the International 2002 Conference on Control Applications*, 2002, pp. 367-372.
- [13] I. M. Horowitz, "Synthesis of Feedback Systems with Nonlinear Time-varying Uncertain Plants to Satisfy Quantitative Performance Specifications," *IEEE Proc.*, **64**, 1976, pp.123-130.
- [14] I. M. Horowitz, "Feedback Systems with Nonlinear Uncertain Plants," *Int. J. Control*, **36**, pp. 155-171, 1982.
- [15] I. M. Horowitz, *Quantitative Feedback Design Theory (QFT)*, **vol. 1**, QFT Publications, 1993.
- [16] C. H. Houpis, and P. R. Chandler, "*Quantitative Feedback Theory Symposium Proceedings*," WL-TR-92-3063, August, 1992.
- [17] C. H. Houpis, S. J. Rasmussen and Mario Garcia-Sanz, *Quantitative Feedback Theory – Fundamentals and Applications* (1st and 2nd editions), Taylor & Francis, 2005.
- [18] H. Jeong, "Structure and Dynamics of Complex Networks," Plenary Lecture, *Complex '07*, Gold Coast, Australia, July 2-4, 2007.
- [19] A. Khodabakhshian and N. Golbon, "Design of a New Load Frequency PID Controller using QFT," *Proceedings of the 13th Mediterranean Conference on Control and Automation*, June, 2005, pp. 970-975.
- [20] W. E. Leland, M. S. Taqqu, W. Willinger, and D. V. Wilson, "On the Self-similar Nature of Ethernet Traffic," *IEEE/ACM Transactions on Networking*, **2**(1), 1994, pp.1-15.
- [21] J. Lyons, J. Ritter, K. Thomas, K. Militello, and P. Vincent, "Collaborative Logistics: Developing a Framework to Evaluate Socio-Technical Issues in Logistic-based Networks," *Proceedings of the 2006 IEEE International Symposium on Collaborative Technologies and Systems*, May 14-17, 2006, pp. 208-214.
- [22] B. B. Mandelbrot: *The Fractal Geometry of Nature*, Lecture notes in Mathematics, W. H. Freeman, San Francisco, 1982.
- [23] J. Moffat, *Complexity Theory and Network-Centric Warfare*, CCRP Publication, 2003.
- [24] N. Niksefat and N. Sepehri, "Designing Robust Force Control of Hydraulic Actuators Despite Systems and Environmental Uncertainties," *IEEE Control Systems Magazine*, April, 2001, pp. 66-77.
- [25] K. B. Oldham and J. Spanier, *The Fractional Calculus*, Academic Press, 1974.

- [26] D. W. Repperger and L. Rothrock, "Using GA-based Intelligent Control Means to Enhance Human-Machine Interfaces," *Auto-Soft – Intelligent Automation and Soft Computing*, vol. 11, No. 2, 2005, pp. 123-140.
- [27] D. W. Repperger, "Evolutionary Algorithms with Application to Biomedical Engineering," book chapter, *Encyclopedia of Biomedical Engineering*, Wiley, Vol. 3, April, 2006, pp. 1519-1528.
- [28] D. W. Repperger, A. R. Pinkus, J. A. Skipper, C. D. Schrider, "Object recognition via information-theoretic measures/metrics," *Proceedings of the IS&T / SPIE's XIX Annual Symposium on Electronic Imaging*, 2007, San Jose, CA., vol 6498, pp. 649802-1-12.
- [29] D. W. Repperger, C. A. Phillips, R. L. Ewing, J. B. Lyons, "Performance of Complex Networks Using Information-Theoretic Means," *The Ohio Journal of Science*, vol. 107(1), pp. A-31, April, 2007.
- [30] D. W. Repperger, R. L. Ewing, J. B. Lyons, R. G. Roberts, "Investigation of Performance of Distributed Complex Systems Using Information-theoretic Means and Genetic Algorithms," *Proceedings of The 7th IEEE International Symposium on Computational Intelligence in Robotics and Automation*, CIRA 2007, Jacksonville, Florida, June 20-23, 2007, pp. 137-142.
- [31] D. W. Repperger, R. G. Roberts, J. B. Lyons, and R. L. Ewing, "Optimization of an Air Logistics System via a Genetic Algorithm Model," under review, *International Journal of Logistics Research*, 2008.
- [32] J. Seyba, J. Lyons, and D. Ames, "Computer-based Aerial Port Simulation (CAPS): Designing an Experiment Examining Team-based Logistics Collaboration," *Proceedings of the 2006 IEEE Int. Symp. on Collaborative Technologies and Systems*, May, 2006, pp. 226-231.
- [33] C. E. Shannon, "Communications in the Presence of Noise," *Proceedings of the IRE*, 37, pp. 10-22, 1949.
- [34] T. B. Sheridan and W. R. Ferrell, *Man-Machine Systems: Information, Control, and Decision Models of Human Performance*, The MIT press, Cambridge, Mass., 1981.
- [35] B. J. West, "Fractal Physiology, Complexity, and the Fractional Calculus," Chapter 6, in *Fractals, Diffusion and Relaxation in Disordered Complex Systems*, in *Advances in Chemical Physics*, vol 133, part B, John Wiley, 2006, Eds. W. T. Coffey and Y. P. Kalmykov.
- [36] D. G. Wheaton, I. M. Horowitz, and C. H. Houpis, "Robust Discrete Controller Design for an Unmanned Research Vehicle (URV) Using Discrete Quantitative Feedback Theory," *1991 NAECON*, May, pp. 546-552.
- [37] S-F Wu, M. J. Grimble, and W. Wei, "QFT Based Robust/Fault Tolerant Flight Control Design for a Remote Pilotless Vehicle," 1999, *Proceedings of the International Conference on Control Applications*, pp. 57-62.

